Optoelectronic Simulation and Optimization of Unconstrained Four Terminal Amorphous Silicon/Crystalline Silicon Tandem Solar Cell

William Taube Navaraj[a,b,c,*], Beerendra Kumar Yadav[a], Anil Kumar[a,b]
[a]Sensors and Technology Group,
CSIR-Central Electronics Engineering Research Institute, Pilani, India
[b]Academy of Scientific and Innovative Research (AcSIR), India.
[c]Electronics and Nanoscale Engineering Division, College of Science and Engineering, University of Glasgow, UK.
*williamtaube@gmail.com

Abstract— Optoelectronic two dimensional (2D) technology computer aided design (TCAD) simulation of unconstrained four terminal hydrogenated amorphous silicon/crystalline silicon (a-Si:H/c-Si) tandem solar cells have been carried out. Tandem solar cell approach is one of the promising approaches to achieve high efficiency solar cell by reducing lattice thermalization loss, but needs extensive optimization as the efficiency depends on a number of parameters. The optoelectronic properties of various materials involved have been taken into consideration and a range of parameters such as top ARC (anti reflection coating) thickness, bottom ARC thickness, a-Si:H solar cell thickness, optical connecting layer thickness, a-Si:H solar cell doping, crystalline silicon solar cells doping etc. have been optimized. The optimization resulted in a simulated efficiency of 19.29% for an untextured planar solar cell.

Keywords—TCAD, silicon tandem solar cells, amorphous silicon, crystalline silicon, optimization.

I. Introduction

The power conversion efficiency of the widely used crystalline silicon solar cells is limited by different losses, namely, reflection, thermalization, contact and recombination. Among the different losses, thermalization losses accounts for more than 40% of the efficiency loss. One among the well-proven concepts to reduce the lattice thermalization loss is the concept of tandem solar cell. Among state-of-the-art solar cells, "Solarjunction^{TM}" has achieved an efficiency of 44.4% in multijunction tandem solar cells with complex materials like GaAs, InGaP, InGaAs[1]. The maximum efficiency achieved by single junction silicon solar cell is 25% with a PERL (Passivated Emitter Rear Locally Diffused) approach [2-4]. Efficient silicon based tandem solar cells are promising candidates, which would address both the cost and efficiency issues. In case of silicon based tandem solar cells, the state-of-the-art is a-Si:H/µC-Si:H tandem solar cell (also called as micromorph solar cell) by Yamamoto et al. with an initial power conversion efficiency of 14.7%[5]. Tokyo Electron ltd. (TEL) Solar demonstrated a micromorph technology solar cell having a stabilized efficiency of 13.1% in cell level and modular efficiency of 12.24%[6,1]. Silicon Tandem Solar Cells of SiQDs (Silicon Quantum Dots) embedded in a dielectric matrix have a shortcoming of very low short circuit current density of a few microamperes and hence are currently not promising with a need for extensive research [7]. HIT(Heterojunction with Intrinsic Thin layer) solar cells, where a c-Si/a-Si:H heterojunction is used are increasingly becoming popular and their efficiency has reached up to 25.6% [1].

a-Si:H/c-Si tandem solar cells are theoretically more promising alternative but much less explored. These tandem solar cells can be configured as both non-series constrained and series constrained. Two-junction tandem solar cells, with a bottom cell of Eg 1.1eV and top cell of 1.8eV, can have a theoretical efficiency approaching 40% under one-sun intensity[8] and non-current constrained mode. According to the theoretical modeling, done by Brown et al. [9], an efficiency of 45.7% is achievable with an unconstrained tandem solar cell with the bottom cell's bandgap 0.95eV and the top cell as 1.74eV. Further, under a series constrained condition with a bottom cells band gap of 0.94eV and the top cell of 1.61eV a 45.3% efficiency is achievable under AM1.5G irradiance [9]. Matsumoto et al. [10] have fabricated a-Si/Poly-Si tandem solar cell with constrained two-terminal and unconstrained four-terminal and have achieved efficiencies of 15.04% and 16.8% respectively. However, these solar cells need extensive simulation based optimization in order to get the best efficiency, which depends on a number of parameters such as top ARC thickness, bottom ARC thickness, a-Si:H solar cells thickness, optical connecting layers thickness, a-Si:H solar cells doping, crystalline silicon solar cells doping profile, etc. In this paper, an extensive simulation of a-Si:H/c-Si tandem solar cells has been carried out using Silvaco^{TM} TCAD software [3], one of the state-of-the-art process and device simulators. Giuseppe Ali et al. have used genetic algorithm with Sentaurus^{TM} TCAD simulator to optimize photovoltaic cells [11]. To the best of our knowledge, there are no known reports on this type of a-Si:H/c-Si tandem solar cells simulation work reported in the literature. The best possible material and physical models for simulation of the silicon tandem solar cell have been considered. In the following section, the device structure, physical models such as mobility, band gap, optical absorption and propagation, defects, and other considerations used in the simulation are explained.

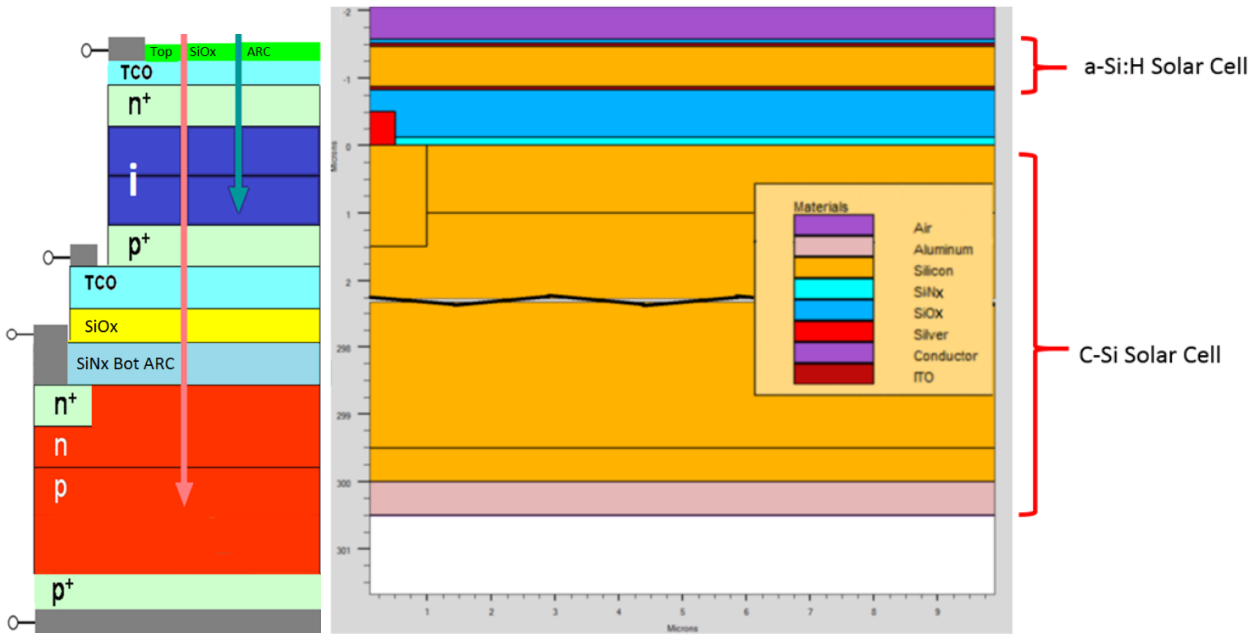

1a 1b

Figure 1: (a) Schematic and (b) Simulation cross-section of typical non-current-constrained four terminal a-Si:H/c-Si tandem solar cell (Dimensions of layers are subject to optimization)

II. Device Structure, Model and Simulation

Figure 1a and 1b shows the schematic and the simulation cross section of the a-Si:H/c-Si Tandem Solar Cell structure respectively. The simulation has been carried out in the Silvaco™ ATLAS TCAD package. The structure consists of an amorphous silicon (a-Si:H) solar cell realized on top of a crystalline silicon (c-Si) solar cell, optically coupled but electrically isolated with each other by a Silicon Oxide (SiO_x) layer. The various models considered for c-Si are; concentration dependent Shockley Read Hall (SRH) recombination, concentration dependent mobility and auger recombination. For a-Si:H, electron and hole mobility of 1 and 0.1 $cm^2/V\text{-}s$ has been considered respectively. A defect states dependent SRH carrier recombination model has been considered. The defect states have been modeled by a thin film transistor (TFT) model of acceptor and donor bump and tail state density as given in figure 2. Effective room temperature conduction and valence band density of states have been taken as 2.5×10^{20} $/cm^3$ for both. An electrical band gap of 1.9 eV has been considered for a-Si:H while 1.12eV has been considered for c-Si. A 1000 μΩ-cm resistivity has been considered for indium tin oxide (ITO). The wavelength-dependent real n and imaginary part k of refractive index for all the materials used such as a-Si:H, ITO, c-Si, Ag, Al, have been taken from SOPRA database. Transfer Matrix Method (TMM) has been used for considering thin film coherence/interference effect as a majority of the layers thicknesses are of the order of the wavelength of the light [12]. AM1.5G spectrum has been considered for simulating the illuminated IV characteristics. However, textures are not considered and the structure has been taken as planar due to simulation constraints. However, the effect of complete light trapping (corresponding to 100% absorption) is discussed later. A surface recombination velocity of 1×10^5 cm/s has been considered for the entire semiconductor/dielectric interface. However, it should be noted, that ideal ohmic contact has been considered and due to this, spreading resistance/contact resistance effects are negligible in the simulation. The device width considered for the 2D simulation is 10 μm as shown in figure 1b.

Table 1 gives the initial structure and doping parameters considered for the simulation.

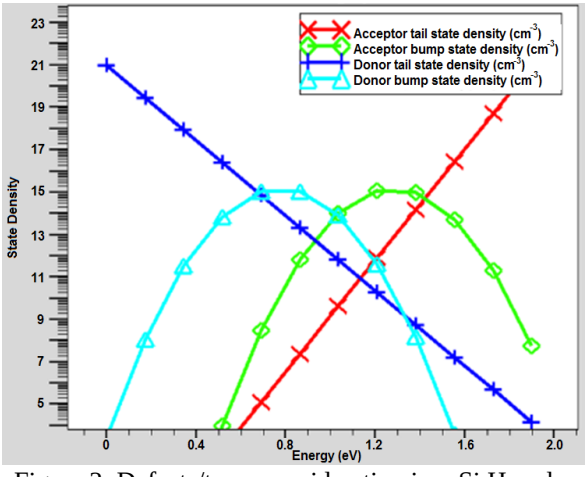

Figure 2: Defects/traps consideration in a-Si:H under TFT model in terms of acceptor and donor bump and tail state density [9][11]

TABLE I. INITIAL SIMULATION PARAMETERS

S. No.	*Parameters*	*Value*	*Unit*
1	Top ARC Si Oxide Thickness	0	nm
2	Bottom ARC Si Nitride Thickness	70	nm
3	Top ITO Thickness	50	nm
4	Bottom ITO Thickness	50	nm
5	a-Si:H N+ Thickness	20	nm
6	a-Si:H Total Thickness	2000	nm
7	a-Si:H P+ Thickness	20	nm
8	a-Si:H Intrinsic Concentration	1×10^{14}	$/cm^3$
9	a-Si:H P+ Concentration	1×10^{20}	$/cm^3$
10	a-Si:H N+ Concentration	1×10^{20}	$/cm^3$
11	a-Si:H Electron lifetime	1	µs
12	a-Si:H Hole lifetime	0.1	µs
13	c-Si Electron lifetime	10	µs
14	c-Si Hole lifetime	10	µs
15	c-Si P+ Concentration	1×10^{19}	$/cm^3$
16	c-Si N+ Concentration	1×10^{20}	$/cm^3$
17	c-Si P Concentration	1×10^{15}	$/cm^3$
18	c-Si N Concentration	1×10^{15}	$/cm^3$
19	c-Si P+ Thickness	0.5	µm
20	c-Si N+ Thickness	1.5	µm
21	c-Si N Thickness	0.5	µm
22	c-Si P Wafer Thickness	300	µm
23	Isolation SiOx Thickness	1000	nm

Initially the a-Si:H thickness has been varied from 50 nm to 3000 nm. Illuminated current density-voltage (J-V) curves were obtained for each case by dividing the current output with the area of the cell i.e. 10 μm^2 (1 µm is considered as 3D width by the 2D TCAD simulator). From the illuminated J-V, the maximum power density (maximum power per square centimetres, mW/cm^2) has been extracted for each thickness, for both the top a-Si:H cell and the bottom c-Si cell. As the thickness of the a-Si:H region is increased it is observed that the maximum power density ($MPD_{a\text{-}Si:H}$) of the a-Si:H solar cell continuously increases and then gets almost saturated to ~11 mW/cm^2 above 1 µm. This is due to increased photons absorption and power conversion within the a-Si:H region. But, increased photon absorption (of energy $E_{h\upsilon\text{-}photon} > E_{g\ a\text{-}Si:H}$) in the a-Si:H region will cause a decreased availability of photons in the c-Si region. This is because, only photons (of energy $E_{h\upsilon\text{-}photon} > E_{g\ c\text{-}Si}$) transmitting through the a-Si:H cell will get absorbed in the c-Si cell resulting in electron-hole pair generation there. So, the c-Si cell's MPD ($MPD_{c\text{-}Si}$) shows a decreasing trend and then a lower saturation to ~4 mW/cm^2 complementing the a-Si:H cells maximum power density trend. Photons with energy $E_{h\upsilon\text{-}photon} < E_{g\ c\text{-}Si}$ will not contribute to the carrier generation in the tandem cell. The initial increase (for <50nm a-Si:H thickness) in the ($MPD_{c\text{-}Si}$) could be attributed to the increased absorption due to the coherence effect arising from the thin a-Si:H region, acting like bottom layer of an ARC along with the top SiO_x ARC. The bottom subplot of figure 3 shows the trend of total tandem efficiency (TTE) with a change in the a-Si:H region's thickness.

The following equation gives the TTE:

$$TTE\ \% = \frac{\mathrm{MPD}_{\mathrm{a-Si:H}}\left(\frac{mW}{cm^2}\right) + \mathrm{MPD}_{\mathrm{c-Si}}\left(\frac{mW}{cm^2}\right)}{AM1.5G\ Power\ Density\ \left(\frac{mW}{cm^2}\right)} x100$$

$$= \frac{\mathrm{MPD}_{\mathrm{a-Si:H}}\left(\frac{mW}{cm^2}\right) + \mathrm{MPD}_{\mathrm{c-Si}}\left(\frac{mW}{cm^2}\right)}{100\ \left(\frac{mW}{cm^2}\right)} x100$$

$$= \mathrm{MPD}_{\mathrm{a-Si:H}} + \mathrm{MPD}_{\mathrm{c-Si}}$$

The maximum TTE has been obtained as 15.61% at 600nm a-Si:H cell's thickness with $MPD_{a\text{-}Si:H}$ and $MPD_{c\text{-}Si}$ of 10.69 mW/cm^2 and 4.92 mW/cm^2 respectively.

An oxide layer has been considered on top of the a-Si:H cell as an Anti-Reflection Coating (ARC). The thickness of the top layer has been varied from 0 nm to 100 nm with a step size of 10nm. As shown in figure 4, without an ARC, the

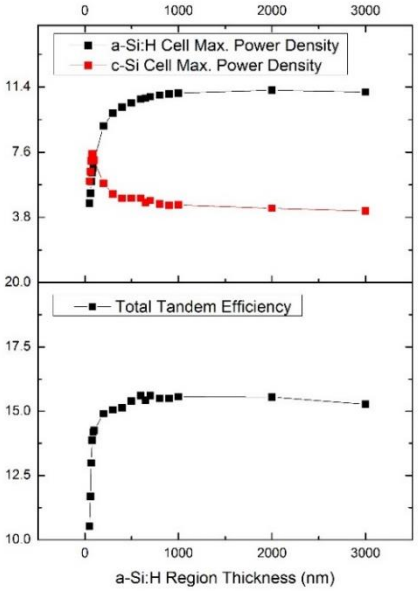

Figure 3: Effect of change in a-Si:H region thickness

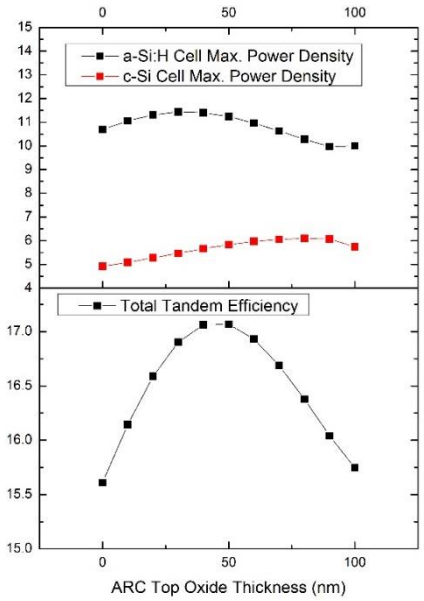

Figure 4: Effect of change in thickness of oxide ARC of top a-Si:H cell

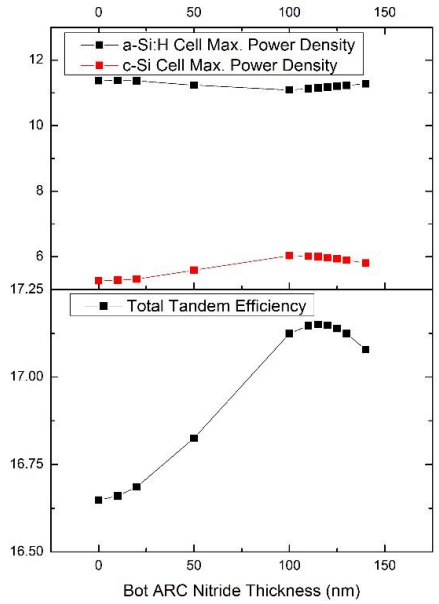

Figure 5: Effect of change in thickness of Nitride ARC of Bottom c-Si Cell

TTE obtained is 15.61%. As the oxide thickness is increased the TTE initially increases to a maximum of 17.07% at 50nm and then decreases to 15.75% at 100nm. This may be explained as follows. For lower thicknesses from 0 to 30nm, the ARC is effective towards photons of the blue end of the solar spectrum, as observed from the increase in efficiency of $MPD_{a\text{-}Si:H}$ to 11.43 mW/cm^2 from 10.69%. After this, as the ARC thickness is increased further (30nm to 80nm) it becomes effective for the red end of the solar spectrum. Due to this, the $MPD_{a\text{-}Si:H}$ decreases while the $MPD_{c\text{-}Si}$ increases. Together, the best TTE (17.07%) is obtained at a thickness of 50nm. An additional silicon nitride ARC has been considered on the top of the bottom crystalline silicon solar cell instead of a double layer ARC on the top. Initially, SiO_x/SiN_x double layer ARC has been attempted on the top. However, it was found that the top cell's short circuit current density (J_{sc}) and MPD increases at the expense of the bottom cells' MPD resulting in lesser TTE from 17.07% at 0 nm SiN_x to 14.69% at 50 nm SiN_x with a SiO_x thickness of 50nm. A similar decrease was observed with a SiO_x thickness of 100nm. From this it is inferred that an additional silicon nitride ARC on the top of the bottom c-Si solar cell is the optimal structure for a-Si:H/c-Si tandem solar cell instead of a double layer ARC on the top. The coupling SiO_x layer's thickness has a very little influence on the TTE arising from the coherence effect. The TTE has changed from 17.03% at SiO_x thickness of 600 nm to 17.14% at SiO_x thickness of 700 nm then it drops to 17.07% at 1000nm. Figure 5 shows the effect of change in thickness of silicon nitride ARC. As the thickness of the nitride region is increased, the TTE increases from 16.65% at 0 nm to 17.15% at 110 nm. It is observed that due to coherence effects the thickness of the bottom cell's ARC affects the MPD of both top a-Si:H cell as well as bottom c-Si cell. The TTE remains constant on ~17.15% from 110nm to 125nm and then drops back beyond 125nm.

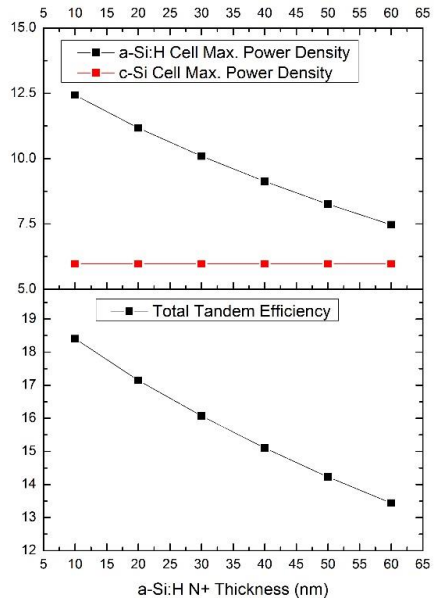

Figure 6: Effect of Change in Thickness of N+ layer of a-Si:H cell

Figure 6 shows the effect of changes in thickness of a N+ layer of a-Si:H solar cell. As the thickness of the N+ layer is increased the TTE decreases from 18.41% at 10 nm to 13.44% at 60 nm. It is observed from the corresponding MPD graph that the c-Si has no role in this change as expected and is constant. It has been found that the change in P+ thickness of a-Si:H solar cell has little effect on the efficiency with 18.45% at 10 nm to 18.36% at 50 nm as shown in Figure 7.

Thicknesses of P+, N+ and N regions of c-Si has negligible influence on the TTE for a range of 0.25 to 2 µm , 0.75 to 2 µm, 0.1 to 2.5 µm respectively with a change of 18.43% TTE to 18.46% for the considered surface recombination velocity in this simulation. For a single

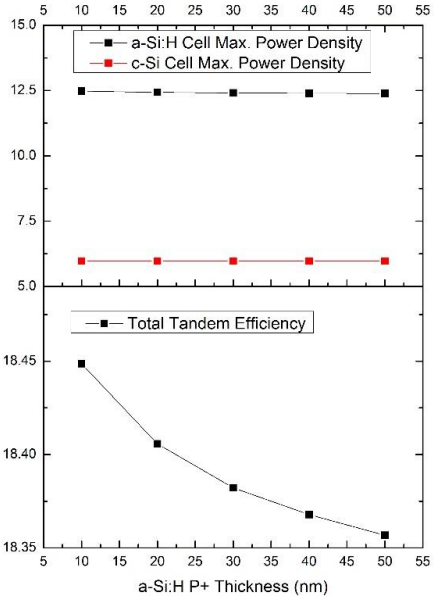

Figure 7: Effect of Change in Thickness of P+ Thickness of a-Si:H cell

junction crystalline silicon solar cell, N+ and N thickness will have a very significant effect because significantly large number of photons (>90%) in blue end of the spectrum gets absorbed close to the top surface of silicon within few µm where the junction is [12]. It is to be noted that crystalline silicon has an absorption coefficient of $>10^5$ /cm for photons of wavelengths less than 480 nm. Hence, the junction profile significantly influences the single junction solar cell's characteristics, especially in the blue region of the spectrum. In the case of a-Si:H/c-Si tandem solar cell, the photons in the blue end are already absorbed in the top cell. The rest of the photons tend to gets absorbed and create most of the carriers in the bulk of the silicon (due to lower absorption coefficient) and hence TTE is not dependent significantly on the N+ thickness and N thickness. Similar effect has been observed in the N region with just a change from 18.45% to 18.46% for a change in concentration from 1e14 to 1e18 /cm^3.

However, bulk P boron doping is found to have a very significant effect in the TTE as observed in figure 8. As expected, it had no effect in the $MPD_{a\text{-}Si:H}$. The $MPD_{c\text{-}Si}$ initially increases as the p-type bulk boron doping is increased, from 17.68 % at 1e14 /cm^3 to 19.1% at 5e16 /cm^3 and then decreases to 17.92% at 1e18 /cm^3.This is because, increasing the base concentration will decrease the base resistance and hence will result in an increase in the open circuit voltage. However, at higher carrier concentration recombination in the quasi-neutral region increases because of lower diffusion length and concentration dependent Shockley-Read-Hall (SRH) recombination. This will result in a decrease in short circuit current density. The optimal concentration was found to be 5e16 /cm^3 corresponding to a p-type boron wafer of resistivity 0.35 Ohm-cm. Optimization of P+ doping

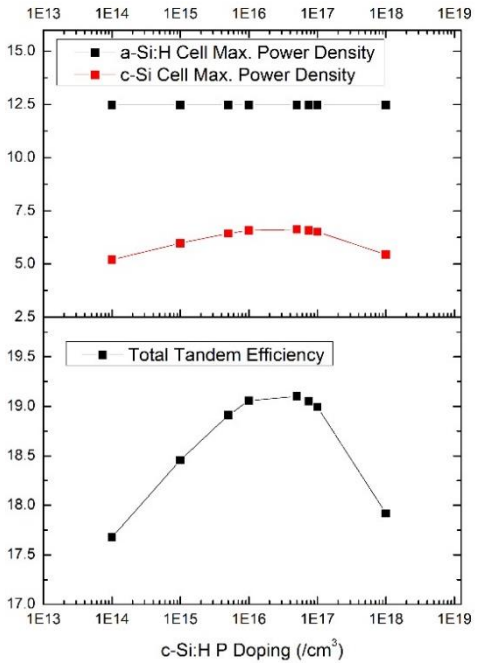

Figure 8: Effect of change in p-type substrate doping concentration of c-Si cell

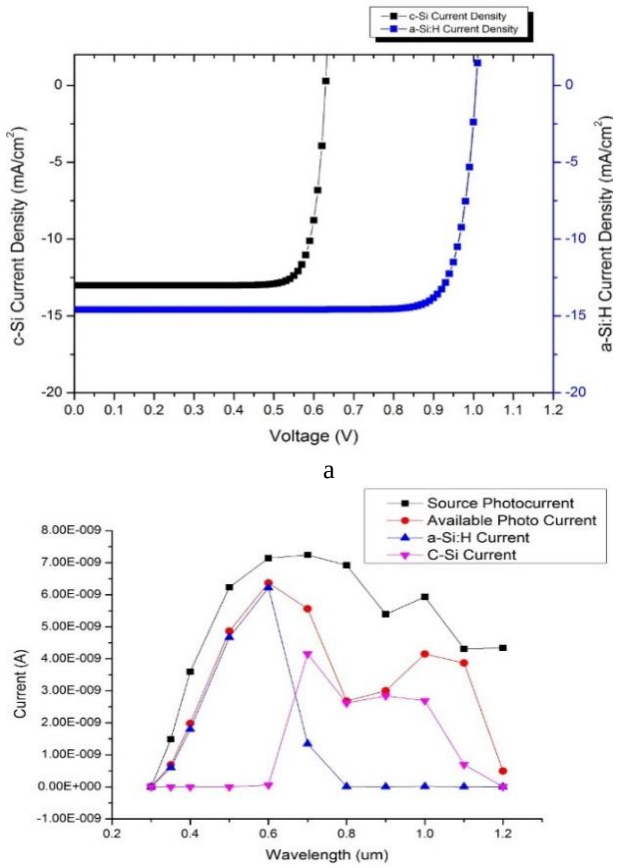

Figure 9 a) J-V characteristics of a-Si:H and c-Si solar cell. b) Source photocurrent, available photocurrent and the a-Si:H and c-Si collected output current.

resulted in a efficiency increase from 19.1% at 1e19 /cm^3 to 19.29% at 1e20 /cm^3.

Figure 9a shows the J-V characteristics of the optimized a-Si:H and c-Si solar cells. The extracted parameters from the J-V characteristics such as doping and structural parameters and device parameters such as short circuit current density (J_{sc}), open circuit voltage (V_{oc}), fill factor (FF) etc. are tabulated in table 2. The a-Si:H solar cell's parameters are compared to an experimental high performance solar cell from literature[13]. The parameters are comparable in value. The Jsc of the experimental solar cell is slightly better than the optimized solar cell due to the improved a-SiC:H p type layer in the experimental cell. The FF in the experimental cell is significantly lower than the designed cell. This is because the experimental cells area is much larger (in several cm2) compared to the simulated cell of just 10µm x 1µm cross section and hence exhibits a series resistance effect. Also, as mentioned earlier, the ITO has been considered to form perfect ohmic contact with a-Si:H in the simulation and hence the lack of series resistance effect results in a higher fill factor.

Figure 9b shows the source photocurrent corresponding to the flux of AM1.5G, available photocurrent and the a-Si:H and c-Si collected current as a function of wavelength. Source

TABLE II. DEVICE PARAMETERS AFTER OPTIMIZATION

Parameters	From Literature (Experimental) [13]	From Our Design Optimization
a-Si:H Solar Cell:		
N-type a-Si:H Thickness	20 nm	10 nm
Intrinsic a-Si:H Thickness	500 nm	600 nm
P-type a-Si:H Thickness	10 nm (a-SiC:H)	10 nm
ITO Layer	100 nm	50nm
a-Si:H Cell Output:		
J_{sc} (mA/ cm^2)	15.94	14.59
V_{oc} (V)	0.993	1.0062
FF	0.674	0.8496
Power Density(mW/cm^2)	10.6	12.476
Other Parameters of Final Cell:		
ARC Top Cell SiO_x Thick		50 nm
ARC Bot Cell SiN_x Thick		120 nm
a-Si:H P+ Conc		$1e20/cm^3$
a-Si:H N+ Conc		$1e20/cm^3$
Intrinsic Conc		$1e14/cm^3$
Coupling SiO_x Thick		700 nm
c-Si:H P+ Conc		$1e20\ /cm^3$
c-Si:H N+ Conc		$1e19\ /cm^3$
c-Si:H P Conc		$5e16\ /cm^3$
c-Si:H N Conc		$1e15\ /cm^3$
c-Si:H P+ Thick		0.5 µm
c-Si:H N+ Thick		1.5 µm
c-Si:H N Thick		1.0 µm
Wafer Thickness		300 µm
c-Si Cell Output:		
J_{sc} (mA/cm^2)		13.0118
V_{oc} (V)		0.63008
FF		0.83117
Power Density (mW/cm^2)		6.81431
TTE %		19.2905%

photocurrent refers to the maximum possible photocurrent at a given wavelength available in the AM1.5G solar spectrum when all the photons at a particular wavelength could undergo electron-hole pair generation, carrier separation and collection at the electrodes. This can be considered as a measure of the rate of photons incident on the device expressed as equivalent current. Available photocurrent refers to the equivalent photocurrent at a given wavelength caused by optical generation, if all the photons which are actually absorbed in the cell regions could undergo electron-hole pair generation, carrier separation and collection. The difference between source photocurrent and available photocurrent is caused by reflection and transmission of photons. Optical efficiency is the ratio between available photocurrent and source photocurrent. Electronic efficiency could refer to either internal quantum efficiency (IQE) or external quantum efficiency (EQE). IQE is given by the ratio between the total photocurrent to the available photocurrent at a given wavelength. EQE is given by the ratio between the total photocurrent to the source photocurrent at a given wavelength. It can be seen that the available photocurrent is significantly lower than the source photocurrent. This is because of higher reflection of the planar structure of the simulated cell. Practically, a textured crystalline silicon solar cell could be fabricated and then on the top of it a a-Si:H solar cell could be realized. Since we have used transfer matrix method for simulation, the effect of texturing could not be directly considered physically. Rather, effect of 100% light trapping has been considered indirectly by multiplying the incident AM1.5G spectrum with wavelength specific scaling factors given as source photocurrent at each wavelength divided by available photocurrent at that particular wavelength. This results in an efficiency of 30.55 %. Figure 10a and 10b shows the JV characteristics and the spectral characteristics of the solar cell considering 100% AM1.5G absorption up to the wavelength corresponding to the band gap of the bottom cell (1.11eV/1.2µm). With texturing the efficiency of the tandem solar cell will fall somewhere in between 19.29% to 30.55 %.

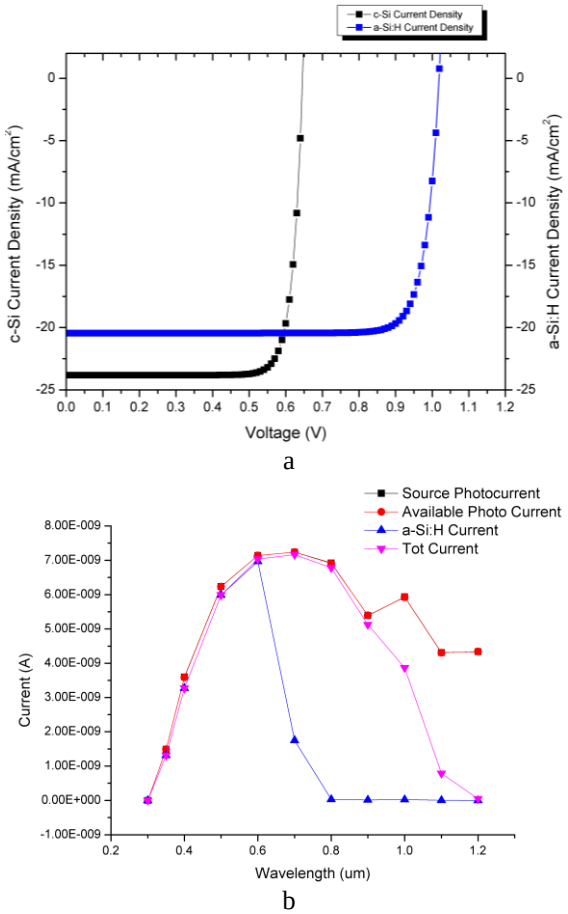

Figure 10 a) J-V characteristics of a-Si:H and c-Si solar cell considering complete AM1.5G light trapping b) Source Photocurrent, 100% trapped AM1.5 G available photocurrent (overlapping with source photocurrent) and the a-Si:H and c-Si collected output current.

III. Conclusion

Unconstrained four terminal amorphous silicon/crystalline silicon tandem solar cell has been optimized using two-dimensional Silvaco™ TCAD simulation. Transfer Matrix Method has been used for considering thin film coherence/interference effects. Optoelectronic properties of various materials involved have been taken into consideration such as bandgap, refractive index from SOPRA database, defects, mobility models etc. and a range of parameters such as top ARC thickness, bottom ARC thickness, a-Si:H solar cells thickness, optical connecting layers thickness, a-Si:H solar cells doping, crystalline silicon solar cells doping etc. have been optimized. The optimization resulted in a simulated efficiency of 19.29% for untextured planar solar cell whereas 30.55% for a cell considering 100% absorption or complete light trapping up to the wavelength corresponding to bandgap of the bottom cell. It is to be noted that the results from simulation are overestimating the efficiency due to effects, which are not taken in to consideration such as ITO spreading/contact resistance effect, carrier recombination at the contacts and radiative recombination within the a-Si:H and c-Si materials[14,15] etc.

IV. Acknowledgment

The authors would like to thank The Director, CSIR-CEERI, Pilani for his motivation and support. This work has been funded under a CSIR network project. The authors would like to acknowledge financial support from CSIR.

References

1. Green, M.A., Emery, K., Hishikawa, Y., Warta, W., Dunlop, E.D.: Solar cell efficiency tables (version 44). Progress in Photovoltaics: Research and Applications **22**(7), 701-710 (2014). doi:10.1002/pip.2525
2. Green, M.A.: The path to 25% silicon solar cell efficiency: History of silicon cell evolution. Progress in Photovoltaics: Research and Applications **17**(3), 183-189 (2009). doi:10.1002/pip.892
3. ATLAS User Manual. (2015).
4. Shaw, J.G., Hack, M.: An analytic model for calculating trapped charge in amorphous silicon. Journal of Applied Physics **64**(9), 4562 (1988). doi:10.1063/1.341258
5. Yamamoto, K., Nakajima, A., Yoshimi, M., Sawada, T., Fukuda, S., Suezaki, T., Ichikawa, M., Koi, Y., Goto, M., Meguro, T., Matsuda, T., Kondo, M., Sasaki, T., Tawada, Y.: A high efficiency thin film silicon solar cell and module. Solar Energy **77**(6), 939-949 (2004). doi:10.1016/j.solener.2004.08.028
6. Ltd., T.E.: New Record-Breaking PV Module Efficiency has been achieved. (2014).
7. Perez-Wurfl, I., Ma, L., Lin, D., Hao, X., Green, M.A., Conibeer, G.: Silicon nanocrystals in an oxide matrix for thin film solar cells with 492mV open circuit voltage. Solar Energy Materials and Solar Cells **100**, 65-68 (2012). doi:10.1016/j.solmat.2011.02.029
8. Noufi, R., Young, D.L., Coutts, T.J., Gessert, T., Ward, J.S., Duda, A., Wu, X., Romero, M., Dhere, R., Abu Shama, J.: Toward a 25%-efficient polycrystalline thin-film tandem solar cell: practical issues. In: Photovoltaic Energy Conversion, 2003. Proceedings of 3rd World Conference on, 18-18 May 2003 2003, pp. 12-14 Vol.11
9. Brown, A.S., Green, M.A.: Detailed balance limit for the series constrained two terminal tandem solar cell. Physica E: Low-dimensional Systems and Nanostructures **14**(1–2), 96-100 (2002). doi:http://dx.doi.org/10.1016/S1386-9477(02)00364-8
10. Matsumoto, Y., Miyagi, K., Takakura, H., Okamoto, H., Hamakawa, Y.: a-Si/poly-Si two- and four-terminal tandem type solar cells. In: Photovoltaic Specialists Conference, 1990., Conference Record of the Twenty First IEEE, 21-25 May 1990 1990, pp. 1420-1425 vol.1422
11. Alì, G., Butera, F., Rotundo, N.: Geometrical and physical optimization of a photovoltaic cell by means of a genetic algorithm. J Comput Electron **13**(1), 323-328 (2014). doi:10.1007/s10825-013-0533-0
12. Piprek, J.: Semiconductor optoelectronic devices: introduction to physics and simulation. Academic Press, (2003)
13. Guha, S., Yang, J.: High-efficiency amorphous silicon alloy based solar cells and modules. (2005).
14. Murayama, K.: Hopping and radiative recombination at localized band tail states in hydro- genated amorphous silicon. physica status solidi (c) **8**(1), 198-204 (2011). doi:10.1002/pssc.201000558
15. Nguyen, H.T., Baker-Finch, S.C., Macdonald, D.: Temperature dependence of the radiative recombination coefficient in crystalline silicon from spectral photoluminescence. Applied Physics Letters **104**(11), 112105 (2014). doi:10.1063/1.4869295